JACS
JOURNAL OF THE AMERICAN CHEMICAL SOCIETY
Article
pubs.acs.org/JACS

# Interplay between Structure and Relaxations in Perfluorosulfonic Acid Proton Conducting Membranes

Guinevere A. Giffin,[†] Gregory M. Haugen,[‡] Steven J. Hamrock,[‡] and Vito Di Noto*[,†]

[†]Department of Chemical Sciences, University of Padova, Via Marzolo 1, I-35131 Padova, Italy
[‡]3M Fuel Cell Components Group, 3M Center, St. Paul, Minnesota 55144, United States

Supporting Information

**ABSTRACT:** This study focuses on changes in the structure of ionomer membranes, provided by the 3M Fuel Cells Component Group, as a function of the equivalent weight (EW) and the relationship between the structure and the properties of the membrane. Wide-angle X-ray diffraction results showed evidence of both non-crystalline and crystalline ordered hydrophobic regions in all the EW membranes except the 700 EW membrane. The spectral changes evident in the vibrational spectra of the 3M membranes can be associated with two major phenomena: (1) dissociation of the proton from the sulfonic acid groups even in the presence of small amounts of water; and (2) changes in the conformation or the degree of crystallinity of the poly(tetrafluoroethylene) hydrophobic domains both as a function of EW and membrane water content. All the membranes, regardless of EW, are thermally stable up to 360 °C. The wet membranes have conductivities between 7 and 20 mS/cm at 125 °C. In this condition, the conductivity values follow VTF behavior, which suggests that the proton migration occurs via proton exchange processes between delocalization bodies (DBs) that are facilitated by the dynamics of the host polymer. The conductivity along the interface between the hydrophobic and hydrophilic domains makes a larger contribution in the smaller EW membranes likely due to the existence of a greater number of interfaces in the membrane. The larger crystalline domains present in the higher EW membranes provide percolation pathways for charge migration between DBs, which reduces the probability of charge transfer along the interface. Therefore, at higher EWs although there is charge migration along the interface within the hydrophobic−hydrophilic domains, the exchange of protons between different DBs is likely the rate-limiting step of the overall conduction process.

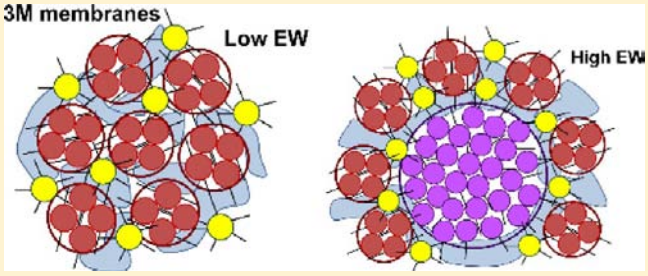


## INTRODUCTION

Proton exchange membrane fuel cells (PEMFCs) are advantageous for energy conversion technologies because they are compact, lightweight and have high power densities with high current densities as compared to some of the other families of fuel cells.[1,2] Despite promising gains in research, development, and implementation, there are still several important technological and economic barriers that must be overcome before the widespread commercialization of fuel cells can occur. One such barriers lies in the production of proton exchange membranes that exhibit high chemical, electrochemical and thermal stability, low reactant permeability, high proton conductivity and low production costs.[3−6] Membranes currently account for 40% of the fuel cell stack cost at low volume.[5] In addition, most available materials can only be used in limited operating conditions and suffer from chemical and mechanical durability issues.[5] The U.S. Department of Energy has set specific goals for 2017 for new membranes such as a low area specific resistance (0.02 Ω·cm$^2$) at the targeted operating conditions of high temperature (120 °C) and low relative humidity (40−80 kPa $P_{water}$) and the cost must be reduced to 20 USD/m$^2$.[5]

The research into development of novel membranes has been directed toward several different classes of materials including perfluorinated, aromatic and hybrid composite membranes. Despite many years of research, perfluorosulfonic acid (PFSA) membranes remain the most effective membranes. There are several commercially available PFSAs, including Nafion (Dupont), Flemion, (Asahi Glass), Aciplex (Asahi Kasei), Aquivion (Solvay Solexis), and the 3 M membrane. These materials contain nonpolar poly(tetrafluoroethylene) (PTFE) main chains and perfluoroether or perfluoroalkyl side chains terminated with $-SO_3H$ groups. The combination of these moieties, which have very different polarities, results in a separation between the polar and nonpolar phases.[7] This phase separation results in nanostructuring in the materials[8−10] that provides pathways for proton conduction through the polar phases and along the interface between the polar and nonpolar phases.[11]

The structure of the 3M membranes[12] is shown in Scheme 1. Varying the index *n* results in membranes with different equivalent weights (EWs) and ion exchange capacities (IEC). Increasing the EW increases the length of the PTFE segments between side chains and decreases both the density of side

**Received:** October 15, 2012
**Published:** December 18, 2012

   dx.doi.org/10.1021/ja3099799 | J. Am. Chem. Soc. 2013, 135, 822−834

**Scheme 1. Chemical Structure of the 3M Membranes**[a]

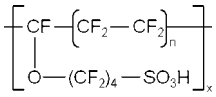

[a]The index $n$ determines the equivalent weight (EW) of the material.

chains and the IEC. Recent studies[13,14] have shown that increasing the EW increases both the crystalline fraction in the polymer and the radius of gyration of hydrophobic domains. Given these morphological changes, it is apparent that a detailed study of the 3M membranes as a function of EW is necessary to correlate the effect of the chemical and structural properties to the physicochemical phenomena occurring in the membrane. This work investigates the thermal, structural, and electrical properties of the 3M membranes as function of EW at different water contents to determine the critical structure–property relationships that affect the conductivity and the operative conditions of the materials.

## EXPERIMENTAL SECTION

**Materials.** The 3M ionomer membranes, provided by the 3M Fuel Cells Component Group (St. Paul, MN), were prepared by casting from a water/alcohol suspension onto a 50 $\mu$m Kapton film. The coatings were then dried at about 110 °C and annealed at 200 °C for about 3 min. The Kapton liner was then removed to provide membranes with a nominal thickness of 25 $\mu$m. These membranes had EWs of 700, 825, 900, 1000, and 1100. The "dry" samples were obtained by drying the polymers for 96 h under vacuum at 90 °C. The "wet" samples were obtained by immersing the samples in double distilled water overnight at room temperature. The "low RH" samples were dried overnight under a dry air flux.

**Instruments and Methods.** Thermal characterization was performed with TG and DSC. TG analyses were performed with a High Resolution TGA 2950 (TA Instruments) thermobalance working under a $N_2$ flux of 100 $cm^3$/min and with a resolution of 1 $\mu$g. A 2920 differential scanning calorimeter (TA Instruments) equipped with a liquid nitrogen cooling system operating under a nitrogen flux of 30 $cm^3$/min with a heating rate of 3 °C/min and a modulation of ±0.95 °C every 60 s in the temperature range from −150 to 350 °C was used to probe the thermal phase transitions. Samples of approximately 4 mg were hermitically sealed in an aluminum pan.

Wide-angle X-ray diffraction (WAXS) patterns were collected in a transmission configuration using a G.N.R. Analytical Instruments Explorer diffractometer in a typical Seeman-Bohling geometry with a Cu K$\alpha_1$ ($\lambda$ = 1.54 Å) source. The diffractometer is equipped with a Johansson-type quartz curved-crystal monochromator aligned on the primary beam. An instrumental 2$\theta$ step of 0.1° with 15 s accumulations was selected. Several pieces of the membrane were layered and sealed between Mylar sheets with silicon grease. The dry membranes were prepared in an Ar atmosphere. A few drops of water were added to the wet samples so that they were maintained at 100% relative humidity at room temperature.

FTIR spectra were collected using a Nicolet FTIR Nexus spectrometer with a resolution of 2 $cm^{-1}$. The spectra of the membranes were obtained in ATR mode with a Perkin-Elmer Frustrated Multiple Internal Reflections 186-0174 accessory.

Electric spectra were measured with BES in the frequency range from 10 mHz to 10 MHz using a Novocontrol Alpha analyzer over the temperature range from −155 to 155 °C. The temperature was controlled using a homemade cryostat operating with an $N_2$ gas jet heating and cooling system. Temperatures were measured with accuracy greater than ±0.4 °C. The membranes were sandwiched between two circular gold electrodes inside a closed cylindrical Teflon cell. The cell was closed to avoid water loss during the measurement of wet samples and water adsorption before the measurement of the dry samples. The estimated pressure inside the sealed cell is in the range from 1 to 5.4 bar for the temperature range from 100 to 155 °C. The geometrical cell constant was determined by measuring the electrode–electrolyte contact surface and the distance between electrodes with a micrometer. Corrections for thermal expansion of the cell were not used.

**Quantum Chemical Calculations.** First-principle calculations were carried out using density functional theory methods implemented in an all-electron DFT code using the DMol3 program[15,16] as a part of the Materials Studio package (double numerical plus polarization basis set, gradient-corrected (GGA) BLYP functional). The 3M side chain was modeled using perfluoro(2-propoxybutane)sulfonic acid. The internal modes were identified by animating the atomic motion of each calculated mode using through features available in the DMol3 package.

## RESULTS AND DISCUSSION

The relationship between the chemical structure and the thermal and electrical properties of the 3M membranes is studied by characterizing the material with several different techniques. The structure is investigated with WAXS and FTIR, while the thermal and electrical properties are studied with TGA, MDSC, and BES. These studies focus on change in the structure as a function of the EW of the polymer and the effect of the structure on the properties of the membrane. The relationship between the index $n$ from Scheme 1 and the EW is shown in eq 1.

$$2n = \frac{(\mathrm{EW} - 328\ \mathrm{g/mol})}{50\ \mathrm{g/mol}} \quad (1)$$

Based on this relationship, EWs of 700, 825, 900, 1000, and 1100 correspond to an average of 8.5, 11, 12.5, 14.5, and 16.5 $CF/CF_2$ moieties in a repeat unit of the 3M PFSA, respectively. Decreasing EW results in shorter PTFE segments between the side chains and a larger number of side chains in a given amount of material.

**WAXS Analysis.** The structural features, and in particular the organization of the polymer chains, can be studied with X-ray diffraction techniques. Diffraction techniques have been extensively used to study structurally similar polymers, e.g. Nafion,[17−19] and the results have permitted the construction of various morphological models.[9,18,20] Small-angle X-ray diffraction (SAXS) has been more widely applied to the study of polymers because it allows the examination of larger structural features. Previous SAXS studies on the 3M membranes have demonstrated that the radius of gyration $R_g$ of hydrophobic crystalline and hydrophilic ionic domains increases from 4.7 to 12.1 and from 25.86 to 34.32 Å, respectively, with increasing EW from 732 to 1082 in the dry membrane.[13,14] This result is consistent with the increased amount of the hydrophobic backbone in the material at higher EW.[13] In addition, the authors suggested that the increased PTFE content also seemed to influence the increased $R_g$ of the hydrophilic clusters.[13]

Based on stoichiometry, the number of PTFE units in a repeat unit can be used to predict which PTFE crystalline structures can possibly contribute to the ordered hydrophobic domains in the 3M membranes. Four structural models, including $2_1$, $15_7$, $10_3$, and $4_1$ helices, have been proposed for PTFE.[21,22] The helical structure of the polymer may be described by $X_t$, where $X$ indicates the number of chemical units distributed in $t$ turns of the helix in the translational repeat units along the chain axis. Therefore, the notation $10_3$ indicates that the translational repeat unit along the helical axis corresponds to 10 $CF_2$ moieties distributed in 3 turns of the helix.[23] If these models are applied to PFSA membranes,


dx.doi.org/10.1021/ja3099799 | J. Am. Chem. Soc. 2013, 135, 822−834

mesoscale ordered structures are only possible when the length of the PTFE segments in the molecular repeat unit corresponds to an integer number of these helical structures. Only in this case would the organization of the side chains have the translational symmetry that is necessary to allow a close packing of the PTFE segments. If there is no correlation between the length of the PTFE segment and the helical chain, then the side chains would spread around the entire surface of the PTFE chain. On this basis, in the 700 EW PFSA the helical structures with the larger periodicities ($15_7$ and $10_3$) will not likely produce ordered structures. In the same sense, for the highest EW materials, the $10_3$ helix will result in the side chains being distributed all around the PTFE chains. These stoichiometric considerations can be used to form the basis for a hypothesis of the structural models which contribute to the ordering of the various peaks found in the XRD diffraction pattern.

The WAXS spectra of both the dry and wet 3M membranes are shown in Figure 1a. The dry spectra are very similar to

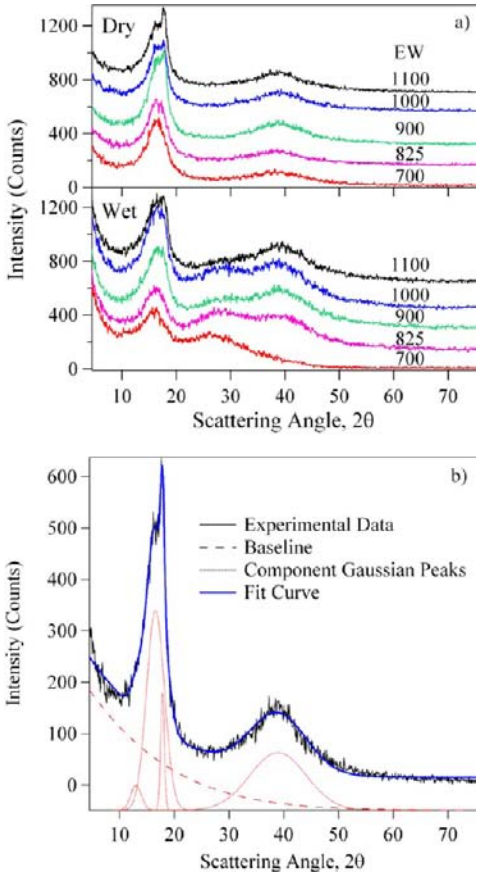


**Figure 1.** (a) WAXS spectra of the 3M membranes with various equivalent weights. The spectra are vertically offset for clarity. (b) WAXS spectrum decomposed with Gaussian peaks. The baseline was subtracted using a broad Gaussian peak.

those previously published for Nafion.[17−19] In Nafion, the intense peak at $2\theta \approx 16.4°$ and the sharp peak at $2\theta \approx 17.7°$ were ascribed to the non-crystalline and crystalline hydrophobic regions of the material, respectively.[17]

The 3M WAXS spectra were decomposed with Gaussian peaks as illustrated in Figure 1b. The background was subtracted using a broad Gaussian peak. The intense peak located between $2\theta$ = 10 and 20° is composed of 2 or 3 overlapping peaks depending on the EW weight located at ca. $2\theta$ = 12.4, 16.4, and 17.7°. In the dry membranes the peak at 17.7°, attributed to the crystalline fraction is present in all EW except the 700 EW material. It is interesting to note that the 3M membranes exhibit crystallinity at EWs where Nafion is amorphous.[24] The absence of the crystalline peak in the 700 EW membrane suggests that a minimum PTFE segment length between adjacent side chains is necessary for the formation of crystalline hydrophobic domains. Based on the EW membranes studied here, it seems that this delimiting chain length is approximately 10 $CF_2$ units between side chains and an EW of approximately 825 g/mol $SO_3H$. This minimum chain length implies that the long-range ordered regions are composed of PTFE helices with longer conformational repeat units. For the 825 EW membrane, this could be the $10_3$ helix, but for all of the other higher EW membranes this is likely the $15_7$ helix. The non-crystalline reflection at 16.4° is likely associated with either the $2_1$ or $4_1$ helices. In addition to these peaks in the 10−20° $2\theta$ range, there is a broad peak at 39° that is associated with ordering of the $CF_2$ units along the polymer chain in the hydrophobic crystalline domains. Although, it cannot be detected in the X-ray pattern, the hydrophobic domains also contain an amorphous fraction. This fraction of material is composed of chains that have no translational symmetry, either due to the presence of random coils or because the arrangement of the side chains prevents ordering. In the higher EW membranes, chains in a $10_3$ helix will likely contribute to this fraction because the side chains will be distributed around the chain.

The crystalline fraction was calculated from the area of the 16.4 and the 17.7° peaks and is shown in the bottom panel of Figure 2. The crystalline fraction is greatest in the 1100 EW

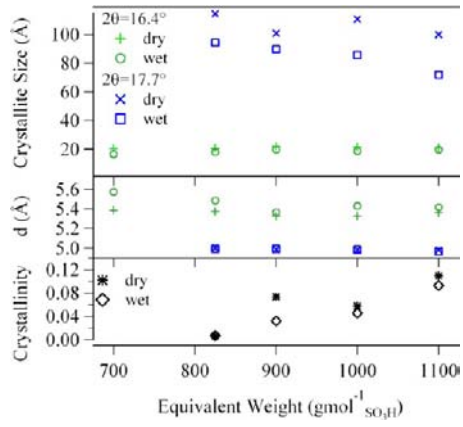


**Figure 2.** Crystallite size, interplanar distance *d*, and crystallinity determined from the WAXS peaks as function of EW.

membrane. The 17.7° peak is smaller in the wet membranes and results of the spectral decomposition, which are in line with the decrease of the peak intensity, demonstrate a reduced crystalline fraction in the wet membrane. This phenomenon is attributed to the removal of chains from the crystallites of the crystalline fraction and may be associated with a conformational transition in the PTFE helices. The Scherrer equation[25] is used to determine the size of the crystallite and the Bragg equation is used to calculate the interplanar distances corresponding to the diffraction peaks. The results are plotted in the top two panels of Figure 2. The non-crystalline reflection (16.4°) corresponds to an interplanar distance, *d*, of 5.3−5.4 Å in both wet and dry conditions. The calculated crystallite size is ca. 20 Å and is


dx.doi.org/10.1021/ja3099799 | J. Am. Chem. Soc. 2013, 135, 822−834

marginally smaller in the wet membrane. These results imply that the morphology of the non-crystalline hydrophobic domains is relatively insensitive to water present within the membrane. The crystalline peak (17.7°) corresponds to an interplanar distance of 5 Å. In dry conditions, this peak corresponds to a crystallite size between 95 and 115 Å and shows no distinct trend as a function of EW. In the wet membrane, the crystallite size is smaller (70−95 Å) and decreases with increasing EW. The interplanar distance calculated for the peak at 39° is 2.3 Å, while the particle size is 6.5−7 Å and 8−9.5 Å in the dry and wet conditions, respectively. This increase in size suggests that water plasticizes the perfluorocarbon chains, which results in a change of the helical pitch and thus the helical conformation.

The interplanar distances for the crystalline and non-crystalline peaks are comparable to those published by Clark[26] for the lateral arrangement of the chain axes in the unit cell of PTFE. Clark states that all forms of the PTFE chain are nearly cylindrical and have nearly hexagonal packing. The data suggest the chains of the 3M membranes in ordered regions primarily exist in small domains that have a diameter of about 20 Å, as shown in Figure 3. However at the higher EWs

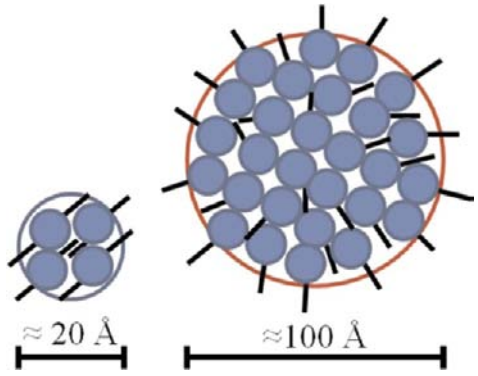


**Figure 3.** Lateral arrangement of chain axes in 3M membranes. This scheme does not contain an appropriate number of chains based on the crystallite size, but is intended to show the morphology of the model only.

where the PTFE segments between side groups are longer, there is also a small amount of larger domains with a diameter of about 95 Å. When there is water in the membrane, some chains are released from the larger domains possibly due to a conformational transition within the chains. As a result, there is a decrease in the size of the larger domains and consequently a decrease in the overall crystallinity.

**Vibrational Spectroscopic Analysis.** The vibrational spectra of the 3M membranes at different water contents are shown in Figure 4. The spectral changes evident in these spectra can be associated with two major phenomena: (1) the dissociation of the proton from the sulfonic acid groups even in the presence of small amounts of water; and (2) changes in the conformation or the degree of crystallinity of the PTFE hydrophobic domains both as a function of EW and membrane water content.

Dissociation of the sulfonic acid proton in Nafion occurs when there is even a small amount of water in the membrane.[27−29] It is reasonable to assume that the differences between the side chain of the 3M membranes and that of Nafion are not sufficient to substantially change the acidity of the sulfonic acid group and therefore dissociation should occur

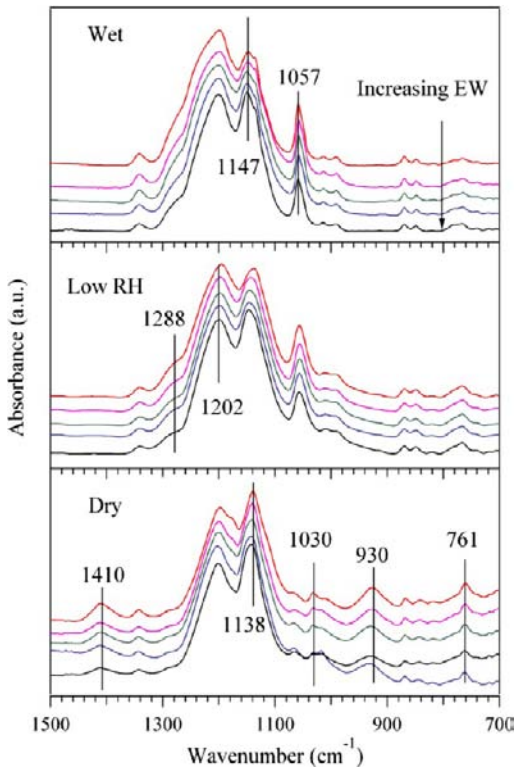


**Figure 4.** FT-IR ATR profiles of the 3M membranes at different water contents. The spectra are vertically offset for clarity with the lowest EW materials at the top and the highest EW membranes at the bottom.

at similar water contents in the 3M materials. The band present at 1410 $cm^{-1}$ is diagnostic of a covalently bound proton in the 3M membranes and is attributed to a mode consisting primarily of $\delta$(SO−H) motion. In this case, this mode will be described as a $\delta$(SO−H) mode. This band was previously observed in other Nafion-containing materials.[30,31] The peak position is constant within the experimental error for all EWs. Even in the "low RH" conditions, the $\delta$(SO−H) mode is no longer visible in the spectrum. A study by Danilczuk et al.[32] calculated the vibrational frequencies for perfluoro(2-ethoxybutane)sulfonic acid that served as a model compound for the 3M side chain. Although this band was not seen in their experimental data, they calculated a vibrational mode associated with a $\delta$(SO−H) motion at 1425 $cm^{-1}$.[32]

In addition to the $\delta$(SO−H) mode, there are several other spectral changes that are characteristic of proton dissociation. The most noticeable of these are the presence of peaks at 930 and 761 $cm^{-1}$ and the very low intensity of the peak at 1059 $cm^{-1}$ in the dry spectrum at all EWs. The peak 930 $cm^{-1}$ is assigned primarily to the $\nu$(C−S) mode of the protonated acid group. DFT calculations published by Warren and McQuillan[33] demonstrated a peak for perfluoro(2-ethoxyethane)sulfonic acid at 971 $cm^{-1}$ that was only present in the acidic form of the model compound. DFT calculations carried out with DMol3 determined that the $\nu$(C−S) motion of perfluoro(2-propoxybutane)sulfonic acid occurred at 912 $cm^{-1}$. The peak at 761 $cm^{-1}$ is attributed to a stretching mode of the oxygen with the covalently bond proton, $\nu$(S−OH). The calculations by Danilczuk et al. found the $\nu$(S−OH) and $\nu$(C−F) motions are mixed at 756 $cm^{-1}$.[32] The DMol3 DFT results of this study produced a mixed $\nu$(S−OH) and $\nu$(C−F) mode at 747 $cm^{-1}$.


dx.doi.org/10.1021/ja3099799 | J. Am. Chem. Soc. 2013, 135, 822−834

The intensity of the 761 $cm^{-1}$ band decreases upon dissociation of the proton but does not completely disappear, which would suggest that when dissociation occurs the resulting single component $\nu$(C−F) band has smaller intensity than the mixed mode. It should be noted that in sulfonic acids the $\nu$(S−OH) mode is decoupled from the $\nu$(S═O) modes of the $SO_2$. In contrast, the modes of the anionic sulfonate are all related to the vibrations of the $SO_3^-$ group. This effect is associated with the charge delocalization due to resonance within the $SO_3^-$ moiety. A careful examination of the DFT results for the acidic model compound confirms that the sulfonate modes of the acidic moiety are essentially divided into two groups: those related to SOH vibrations and the others related to $SO_2$ vibrations.

The low RH and wet samples show an additional band at 1059 $cm^{-1}$ that has a very low intensity in the dry spectrum and originates in the symmetric stretching motion of the $SO_3^-$ group. The growth of this band even at low water contents supports the assumption that the sulfonic acid group of the 3M membranes behaves much like that of Nafion and dissociates in the presence of small amounts of water. When there is one water molecule per sulfonic acid group, the proton dissociates from the $SO_3^-$ moiety to form a hydronium−sulfonate ion-pair. Theoretical results[27−29] have suggested that the proton is not completely dissociated from the sulfonate until $\lambda < 3$. Nevertheless in this work and others[31] in the presence of even very small amounts of water (ca. $\lambda = 1$), FT-IR measurements indicate that the protons are dissociated by the disappearance of the band at 1410 $cm^{-1}$ and the appearance of the band at 1059 $cm^{-1}$. This discrepancy results from a difference in the meaning of dissociation as investigated by FT-IR and theoretical methods. By FT-IR, dissociation of the proton occurs when the covalent bond between the hydrogen and the sulfonate is broken and can be detected by the loss of bands associated with a covalently bound proton and the appearance of peaks attributed to $SO_3^-$ modes. From theoretical methods, several groups[27−29] have illustrated the formation of ion-pairs at $\lambda < 3$, but solvent-separated cations do not occur until $\lambda \geq 3$. After the formation of the hydronium−sulfonate ion-pair as the water content in the membrane increases, the additional water molecules form a solvation sphere around the sulfonate group and the cation moves away from the sulfonate into the bulk of the hydrophilic domains. These two phenomena produce opposite spectral shifts. The formation of a free sulfonate would result in a shift of the $\nu_s(SO_3^-)$ mode to lower frequencies due to the increased electron density in the sulfur oxygen bonds. In contrast, the formation of a solvation sphere around the sulfonate would result in a high frequency shift due to a reduction of the force constant of the sulfur oxygen bonds resulting from the formation of hydrogen bonds with the water molecules. The net result of these opposing phenomena is that there is very little shift in the $\nu_s(SO_3^-)$ peak with increasing water content. As the water content of the membrane increases, the $\nu_s(SO_3^-)$ band narrows because the solvation spheres become more regular in the presence of large amounts of water. Therefore, there is a reduction of the distribution of the hydrogen bonding interactions experienced by the sulfonate and consequently the peak at 1057 $cm^{-1}$ is sharper at higher water content.

Understanding the spectral changes in the broad bands between 1100 and 1300 $cm^{-1}$ is more difficult because they are the result of the superposition of the modes associated with the PTFE-like backbone and the side chain contributions from both the sulfonate mode and the $CF_2$ units. The measurement of the infrared spectra at a low relative humidity (RH) in addition to those in wet and dry conditions helps to separate the spectral changes of the PTFE modes from those of the sulfonate. To make these distinctions, it is assumed that after the addition of small amounts of water (i.e., from dry to low RH conditions), the most significant changes will be associated with the sulfonate modes, while the spectral variations in presence of large amounts of water (i.e., wet conditions) will be primarily due to changes in the PTFE hydrophobic domains. In all EWs, the intensity of the feature at 1138 $cm^{-1}$ decreases with respect to the component at 1202 $cm^{-1}$ and shifts to higher frequency. The initial decrease with the addition of small amounts of water is likely due to the loss of the contribution from a $\nu(SO_2)$ mode associated with the sulfonic acid moiety. This band assignment is supported by the larger decrease in the 700 EW spectra as compared to the higher EW membranes due to the higher number of ion exchange groups present in the membrane. Similar band frequencies have been previously reported for $\nu(SO_2)$ modes in anhydrous organic sulfonic acids.[34] After the loss of the $\nu(SO_2)$ component, further intensity decreases must be associated with changes in the hydrophobic domains. Published FT-IR spectra investigating the thermal transition of PTFE at ca. 20 °C show a large decrease in the band at 1152 $cm^{-1}$ due to the increased disorder in the PTFE chains.[35] On the basis of this result, the subsequent intensity decreases with increasing water content can be associated with the reduction of the crystallinity of the membranes demonstrated from the WAXS results. This loss of crystallinity is likely combined conformational changes that cannot be clearly distinguished here due to the superposition of the spectral features associated with the various helical structures.[21,35] In wet conditions there are at least two significant components contributing to this band (1135 and 1147 $cm^{-1}$) which are associated with different PTFE conformations as previously reported.[21,22] Therefore, these bands can be associated with the ordered PTFE hydrophobic domains (crystalline and non-crystalline as described in the XRD section). In contrast, the band at 1202 $cm^{-1}$ can be associated with the amorphous PTFE fraction.

In dry conditions there is evidence of a small band present at 1176 $cm^{-1}$ that decreases with increasing EW. Based on the vibrational frequencies determined for various models of the PTFE chain conformations,[21,22] this band could be associated with chains in a $4_1$ helical conformation. As discussed above with respect to the WAXS data, this chain conformation is likely present in the non-crystalline ordered domains. As the size of the PTFE chains in the repeat unit decreases, it seems that this conformation becomes less favorable.

The band at 1288 $cm^{-1}$ is likely associated with the $\nu_{as}(SO_3^-)$ mode. Hydration studies of triflic acid showed growth of a band at approximately the same frequency with increasing water content.[36] In dry conditions, this peak has a low intensity that is not dependent on the EW and seems to be proportional to the small feature at 1057 $cm^{-1}$. As water is added to the system, the intensity of the band increases but the size of the growth decreases with increasing EW. The EW dependence of the intensity supports the assignment of this peak to motions associated with sulfonate group.

**Thermogravimetric Analysis.** The thermal stability of the 3M membranes was determined with thermogravimetric analysis and is shown in Figure 5. All of the membranes, regardless of EW, are thermally stable up to 360 °C. This


dx.doi.org/10.1021/ja3099799 | J. Am. Chem. Soc. 2013, 135, 822−834

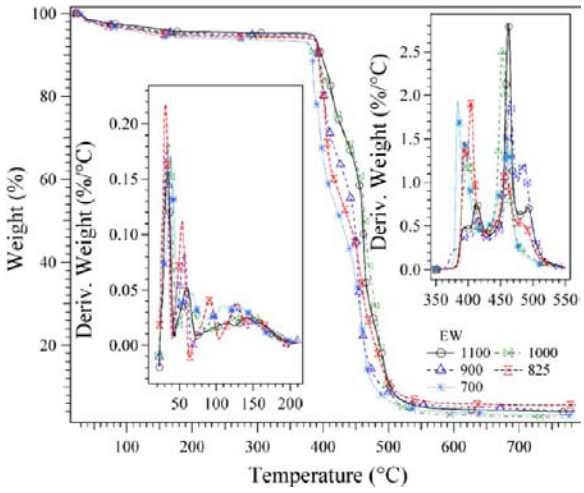


**Figure 5.** TG profiles of 3M membranes with various equivalent weights. The insets show the derivative of the weight percent as a function of temperature.

stability is significantly higher than Nafion, which starts to undergo decomposition between 250 and 300 °C.[30,37] The 3M membranes exhibits a two-step mass elimination at about 360 °C, which is likely due to decomposition of the side chain. The first peak in the derivative curve, which corresponds to the first step, is likely due to the decomposition of the sulfonate group, while the second peak corresponds to the rest of the side chain. The second decomposition at ca. 440 °C, related to the PTFE backbone, quickly follows the first. The increased temperature of the first decomposition as compared to Nafion is likely due to the longer fluorinated butane moiety in the side chain, that behaves more like a short PTFE segment and is therefore more stable than the perfluoroethyl ether found in the Nafion side chain. There are distinct differences between the membranes due to the changes in EW which are particularly evident in an examination of the derivative of the wt%. The first degradation shows two components at all EWs except 1000 EW and these components slowly shift to higher temperatures with increasing EW. This increase in decomposition temperature with increasing EW is likely the result of reducing the number of side chains. The degradation at one side chain site could facilitate decomposition at an adjacent site. In contrast, the decomposition of the main PTFE-like chain is essentially independent of the EW.

At temperatures below 150 °C, there is a small mass elimination that is due to residual water in the membranes. The amount of residual water, which is likely closely associated with the sulfonic acid groups, decreases with increasing EWs. The decreased amount of residual water is not unexpected given that with increasing EW the relative number of side chains, and therefore the number of sulfonic acid groups, decreases. This result is consistent with theoretical studies by Wu et al.[38] Over this range of EWs, the IEC decreases from 1.4 to 0.9 mequiv/g.

**Modulated Differential Scanning Calorimetry.** The thermal transitions are studied using modulated DSC. Two thermal events are evident in the total heat flow MDSC curves of the dry membranes (Figure 6a): one at between −40 and −55 °C and another between 15 and 40 °C. The lower temperature transition, $\beta$, is likely associated with the ether moiety in the side chain. The glass transition of poly(oxytetrafluoroethylene), which has been reported as −48 °C, is comparable with this $\beta$ thermal transition.[39] The $\beta$ event

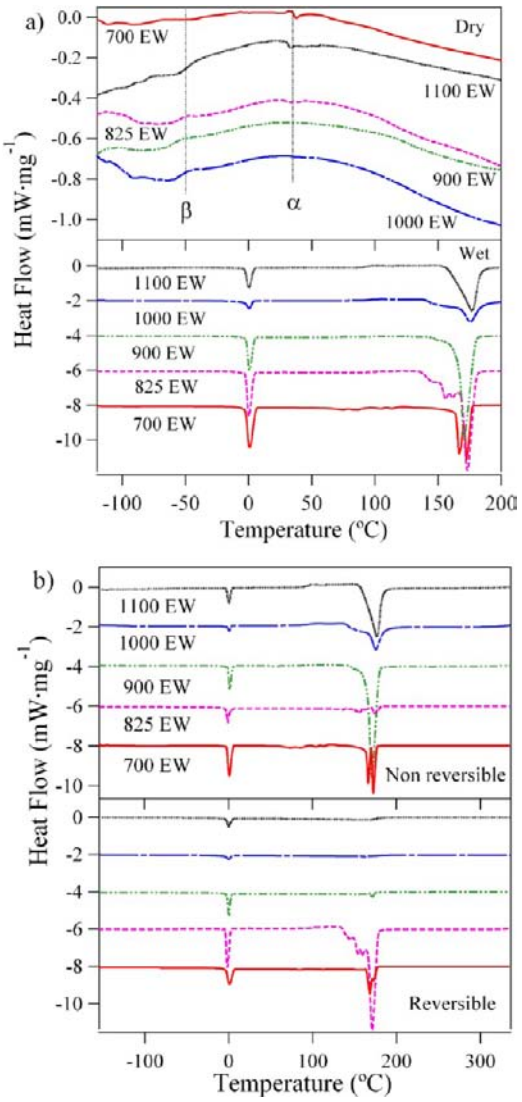


**Figure 6.** (a) MDSC profiles of 3M membranes with various equivalent weights. The wet MDSC curves are vertically offset for clarity. (b) Non-reversible and reversible components of the MDSC profiles. The component curves are vertically offset for clarity.

occurs at −40 °C for the 700 EW membrane and generally decreases in temperature with increasing EW to reach −55 °C for 1100 EW. The higher temperature event, $\alpha$, is assigned to the $13_6 \rightarrow 15_7$ helix transformation and to the order−disorder conformational transitions occurring in hydrophobic PTFE-like domains.[26,30,37] One would expect that this event would be sensitive to the length of the PTFE segments, but there is no clear pattern in the transition temperature as function of the EW length. In addition to the $\alpha$ and $\beta$ transitions, there seems to be a very broad feature starting between 50 and 100 °C. This broad feature is attributed to the $\alpha_{pc}$ transition that is associated with the long-range dynamics of both the backbone and the side chains due to the weakening of electrostatic interactions occurring within the hydrophilic domains.[30,40] The "pc" subscript of $\alpha_{pc}$ indicates that this relaxation mode involves the dynamics of both the hydrophobic and hydrophilic domains of the 3M membranes, unlike the $\alpha$ transition that is associated with the segmental motion of the perfluorinated backbone.[30,40] The thermal transitions occurring in the dry 3M membranes are consistent with those occurring in Nafion.[41]


dx.doi.org/10.1021/ja3099799 | J. Am. Chem. Soc. 2013, 135, 822−834

In the wet membranes, there are two exothermic peaks visible in the MDSC profile. The peak at 0 °C is due to the melting of water. The high temperature peak at ∼170 °C is associated with a relaxation of the PTFE chains. The nature of this relaxation is likely quite complex and may be involved with the melting of small crystalline domains of PTFE hydrophobic domains, chain reorganization, or order−disorder-like transitions that are occurring on a macroscopic scale.[30,37] This event likely shifts to higher temperatures and broadens in the dry membrane due to the size increase of the hydrophobic domains. The reversible and non-reversible heat flow MDSC curves are shown in Figure 6b. In 900 EW polymer and above, the membranes have very little change in the reversible component of the heat flow. Below 900 EW, the membranes have peaks in both the reversible and non-reversible components. This break point would suggest that the larger hydrophobic crystalline domains make a contribution to nonreversible component of this thermal event and influence the behavior of the smaller non-crystalline fractions. The lower EW membranes, 700 and 825, have several significant features, which is indicative of a larger distribution of the small hydrophobic domains due to the much higher density of side chains and is in good agreement with the WAXS results.

**Broadband Electric Spectroscopy.** The electrical properties of the 3M membranes are investigated with broadband electric spectroscopy to determine the polarization and dielectric relaxation events occurring in the materials and subsequently study their associated conductivities, dielectric strengths and relaxation times in both wet and dry conditions. The 3D imaginary permittivity, $\varepsilon''$, surfaces are shown for the 700 and 1100 EW membranes in Figure 7. The real part of the conductivity, the real part of the permittivity and tan $\delta$ for all of the EWs can be found in the Supporting Information (Figures S1−S11). There are three peaks clearly visible in the 700 EW surface: (1) $\beta$, a broad peak that occurs at the lowest temperatures; (2) $\sigma_{EP}$ that has permittivity values greater than $10^2$ and becomes more intense with increasing temperature; and (3) $\alpha$ which has permittivity values less than $10^2$ and is slowly covered by $\sigma_{EP}$ as the temperature increases. The $\beta$ dielectric relaxation is attributed to conformational transitions of the side chain. The $\alpha$ transition is due to the diffusion of conformational states in the PTFE polymer backbone and is associated with the polymer segmental motion. The $\sigma_{EP}$ event, which corresponds to the beginning of a plateau in the real part of the conductivity (Figure S1), is associated with the electrode polarization phenomenon which is the result of the accumulation of charge at the interface between the membrane and the blocking measurement electrodes. In addition to these three peaks, there is a sharp increase in $\varepsilon''$ at high temperature and low frequency attributed to the interfacial polarization, $\sigma_{IP}$. $\sigma_{IP}$ occurs as a result of the accumulation of charge at the interface between regions with different permittivities. If the 3D profile of the 700 EW membrane is compared with that of the 1100 EW membrane, the $\beta$, $\alpha$, $\sigma_{EP}$, and $\sigma_{IP}$ events all seem to be shifted to higher temperatures and another event, $\gamma$, occurs at temperatures lower than those of $\beta$. The $\gamma$ relaxation is due to the local fluctuations of the $CF_2$ units along the PTFE backbone of the 3M membrane. This relaxation is only visible in the 1000 and 1100 EW membranes where the PTFE segments are longer.

The electrical spectra of the wet membranes are much more complicated than those of the dry membranes, particularly in terms of the polarization phenomena. The imaginary 3D

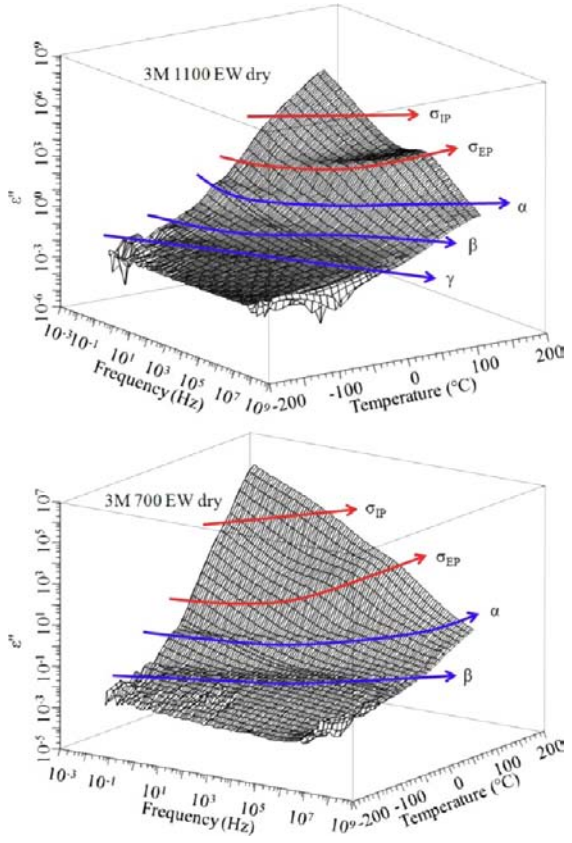


**Figure 7.** 3D surface of the imaginary component of the permittivity for the 700 and 1100 EW dry membranes.

permittivity surfaces for the 700 and 1100 EW membranes are shown in Figure 8. These two spectra show the extremes of the EW range studied, but are generally representative of the behavior across the entire EW range. The spectra can be visibly divided into two temperature regions: above and below the melting point of water at 0 °C. The water phase transition results in a large increase in the intensity of the electrode polarization. The top half of the spectra in Figure 8 details the behavior above the melting point of water. Here, the electrode polarization is the most prominent feature of the spectra. In all membranes, there are two contributions to the electrode polarization immediately above 0 °C that merge into a single peak at higher temperatures. These two features are also evident in the conductivity spectra in Figure 9 as two inflection points that mark the start of the plateau. In the bottom half of the 3D spectra (below the water phase transition), the most prominent feature is the pair of intense peaks that move to higher frequency with increasing temperature. These peaks correspond to the start of a pair of plateaus visible in the real part of the conductivity spectra shown in Figure 9. The higher frequency peak and plateau corresponds to the electrode polarization, while the lower frequency peak is associated with an interfacial polarization. The intense interfacial polarization peak is more clearly separated from the electrode polarization in the spectra of the lower EW membranes. In the higher EW membranes, there is another interfacial polarization that is occurring between the other two polarizations.

Three dielectric relaxations, $\gamma$, $\beta_1$, and $\beta_2$, can be detected in both EW spectra of Figure 8. However, these events are easiest to see in the plot of tan $\delta$ as a function of temperature as shown in Figure 10. As compared to the dry membrane, all of the


dx.doi.org/10.1021/ja3099799 | J. Am. Chem. Soc. 2013, 135, 822−834

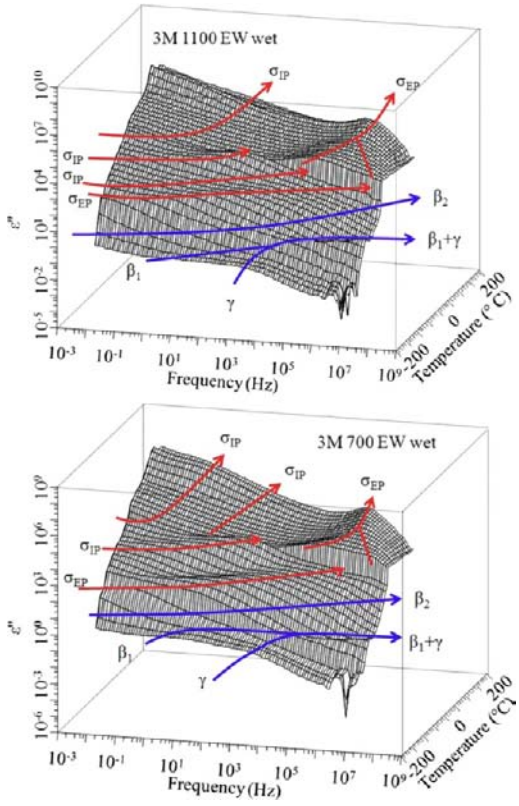


**Figure 8.** 3D surface of the imaginary component of the permittivity for the 700 and 1100 EW wet membranes.

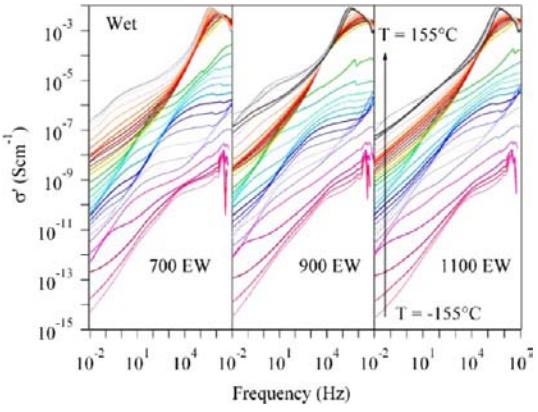


**Figure 9.** The real component of the conductivity for the 700, 900, and 1100 EW wet membranes.

molecular relaxations in the hydrated system are shifted to higher frequencies and lower temperatures due the interaction of non-crystalline water with the sulfonate groups at the interface between the side chains and crystalline water. In addition, the $\beta$ relaxation is now divided into two components, $\beta_1$ and $\beta_2$. The $\beta_1$ mode is assigned to the fluctuation of the dipole of the side chain closer to the backbone, i.e., the ether moiety, while the $\beta_2$ relaxation is associated with the fluctuations of the dipole of the sulfonate group solvated by the water in the membrane. The $\gamma$ relaxation associated with the local fluctuations of the $CF_2$ units in the backbone occurs at approximately −120 °C. The $\beta_1$ and $\gamma$ relaxations are evident in the 3D spectra of Figure 8 as two separate peaks at the lowest temperatures and then merge into a single peak. The $\beta_2$

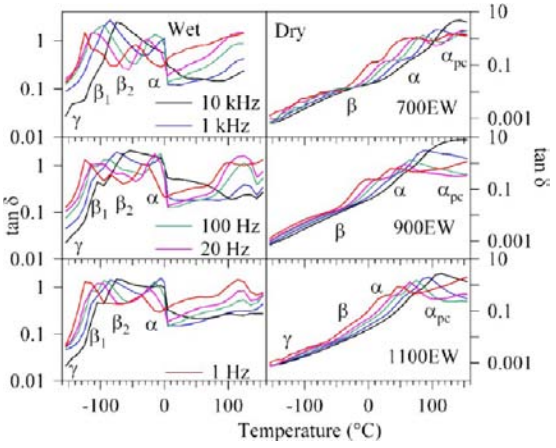


**Figure 10.** Tan $\delta$ as a function of temperature for selected EW materials.

relaxation is harder to discern in the permittivity and conductivity representations because it is partly covered by the electrode polarization. The $\alpha$ relaxation, which was clearly evident in the 3D permittivity spectra of the dry membrane, is now completely covered by the polarization phenomena. However, it is visible in the tan $\delta$ temperature spectra of Figure 10. In highly conductive materials, the molecular relaxations may be detected in the tan $\delta$ curves plotted as a function of temperature because the conductivity is often suppressed in this representation.[42] The $\alpha_{pc}$ relaxation event occurs at approximately 90 °C in the dry membranes.

While the electric spectra of the 3M membranes in wet conditions shown here have some similarities with the spectra previously published for Nafion,[42] the behavior is significantly more complicated, particularly with respect to the polarization phenomena. The 3M spectra are characterized by multiple overlapped contributions, which are mostly easily visualized in the tan $\delta$ spectra as a function of frequency as shown in Figure 11. The various electric polarizations and dielectric relaxations are evident as peaks in the tan $\delta = \varepsilon''/\varepsilon'$ frequency spectra. It is interesting to note that the 900 EW spectra are an intermediate

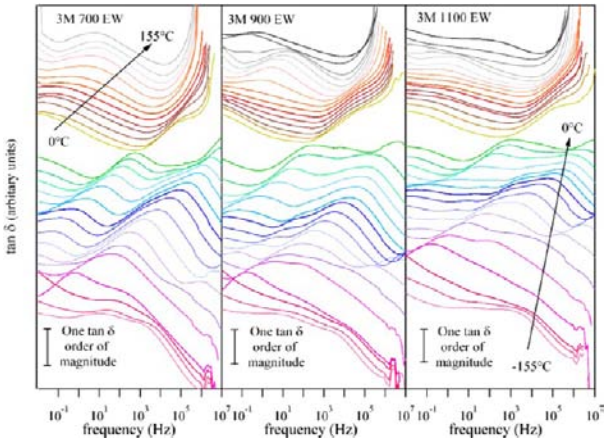


**Figure 11.** Electric tan $\delta$ spectra of the 700, 900, and 1100 EW wet membranes. The spectra are vertically offset for clarity. The temperature increases from −155 °C (bottom) to 155 °C (top) by 10 °C increments. The tan $\delta$ spectra for the 900 EW membrane where the curves are not vertically shifted is shown in the Supporting Information, Figure S11.


dx.doi.org/10.1021/ja3099799 | J. Am. Chem. Soc. 2013, 135, 822−834

between the two extreme EWs. As in the imaginary permittivity spectra, the dielectric relaxations are only seen at the lowest temperatures and quickly move out of the experimental frequency range.

The conductivity values and relaxation times associated with the polarization phenomena and the dielectric strengths and relaxation times associated with the dielectric relaxations can be determined from fitting the experimental $\varepsilon'$ and $\varepsilon''$ data with a general empirical equation:[42]

$$\varepsilon^*(\omega) = i\left(\frac{\sigma(T)}{\varepsilon_0\omega}\right)^{N(T)} + \sum_{k=0}^{3}\frac{\sigma_k(i\omega\tau_k)^{\gamma_k}}{i\omega[1+(i\omega\tau_k)^{\gamma_k}]} + \sum_{j=0}^{1}\frac{\Delta\varepsilon_j}{[1+(i\omega\tau_j)^{\alpha_j}]^{\beta_j}} + \varepsilon_\infty \quad (2)$$

where $\varepsilon^*(\omega) = \varepsilon'(\omega) - i\varepsilon''(\omega)$. The quantity $\varepsilon^*(\omega)$ describes the measured complex permittivity as the superposition of all the phenomena, such as polarization and dielectric relaxation events, characterizing the electrical response of a material.[42] The first term describes the conductivity of the material at frequencies lower than those experimentally measured, while $\varepsilon_\infty$ accounts for the electronic contributions to the permittivity. The second term accounts for the polarization phenomena, where $k = 0$ for the electrode polarization and $k = 1$, 2, or 3 for the interfacial polarizations. The variables $\sigma_k$ and $\tau_k$ are the conductivity and relaxation time associated with the $k$th polarization event, while $\gamma_k$ is a shape parameter that describes the broadening and asymmetry of the $k$th peak. The third term expresses the dielectric relaxation through a Havriliak–Negami relationship[42] where $\omega = 2\pi f$ is the angular frequency of the electric field, $\tau_j$ is the relaxation time of the $j$th event that has an intensity $\Delta\varepsilon_j$, and $\alpha_j$ and $\beta_j$ are shape parameters that account for the symmetric and asymmetric broadening of the $j$th peak. A good fit of the data is achieved when both $\varepsilon'$ and $\varepsilon''$, along with $\sigma''$, $\sigma'$, and tan $\delta$ are reasonably well matched simultaneously.

Charge transport in proton conducting ionomers in general occurs via proton "hopping" processes between coordination sites within the material. The conductivity values determined by fitting the data with the empirical equation given above tend to follow a form that corresponds with either the Arrhenius or Vogel–Tammann–Fulcher (VTF)[43−45] equation shown here:

$$\sigma_i = AT^{-1/2}\, e^{-E_i/R(T-T_o)} \quad (3)$$

where $A$ is a constant proportional to the number of charge carriers, $R$ is the gas constant, $E_i$ is the pseudo-activation energy, and $T_o$ is the thermodynamic ideal glass transition temperature at which the configurational entropy becomes zero or the "free volume" disappears.[46]

If the temperature dependence of the conductivity follows an Arrhenius form, then the conduction mechanism depends only on the temperature and the activation energy; therefore, the protons move via "hopping" processes between coordination sites. The temperature dependence of the conductivity given by the VTF equation was explained in the formalisms of free-volume models or dynamic bond percolation theories (DBPT), which demonstrates that the long-range migration of charge is strongly assisted by the motion of the polymer host matrix and thus by the viscosity of the polymer backbone chains.[46] Therefore, the conduction process occurs via "hopping" processes between coordination sites, where ion exchange is mediated by the segmental motion of the host matrix. VTF behavior can be generalized to any relaxation process that is associated with the segmental motion of the polymer. On the basis of the "free-volume" and DBPT formalisms, when the temperature dependence of either the conductivity or the relaxation frequencies exhibits: (a) Arrhenius behavior, the $E$ in the exponent can be interpreted as the activation energy for either ion motion or the relaxation event; (b) a VTF dependence, the $E$ in the exponent is the "apparent activation energy" (pseudo-activation energy) and should not be considered a true activation energy for either conduction or the relaxation event. In the "free volume model", $E$ is the activation energy that depends on the polymer matrix expansivity[46] and therefore the probability of a large increase in the free volume formation in the bulk matrix for ion migration and relaxation events. In configurational entropy models, the activation energy is related to the "free energy barrier" of the matrix.[46] The conductivity values associated with the interfacial and electrode polarization phenomena determined from fitting the data of the dry membranes are plotted as a function of $1000/T$ in Figure 12. In all EWs, the conductivity

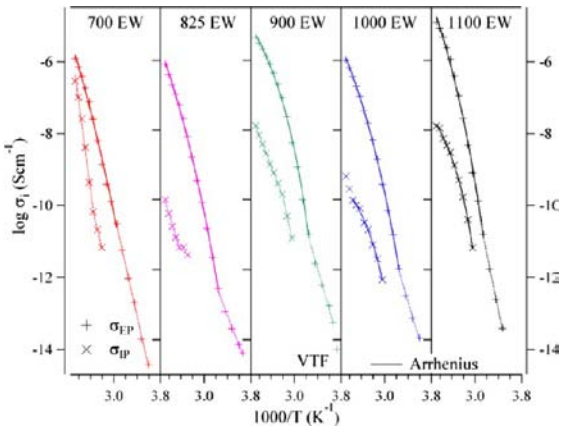


**Figure 12.** Log of conductivity as a function of $1000/T$ for the dry 3M membranes. The plot for the corresponding relaxation frequencies is shown in the Supporting Information, Figure S12.

associated with the electrode polarization, $\sigma_{EP}$, can be divided into two regions at approximately 30 °C, which corresponds to the temperature associated with the $\alpha$ relaxation in the MDSC curves and the BES tan $\delta$ temperature spectra. Below 30 °C, the conductivity $\sigma_{EP}$ follows Arrhenius behavior which implies that the conductivity follows a "hopping" process.[40] Above 30 °C, the $\sigma_{EP}$ follows a VTF form, which indicates that the $\sigma_{EP}$ is facilitated by the dynamics of the polymer chain above the $\alpha$ relaxation of the perfluorinated main chain. The pseudo-activation energies associated with the VTF behavior are approximately 40 kJ/mol for the 700 and 825 EW membranes and 10–25 kJ/mol for the three high EW membranes. The higher activation energy of the lower EW membranes is likely due to the higher number of side chains. A higher number of side chains would likely result in an increased density of dipole–dipole interactions between different chains, which would inhibit the diffusion of conformation states along the shorter PTFE segments between the side chains.

In all equivalent weights except for 700 EW, the conductivity associated with interfacial polarization, $\sigma_{IP}$, is several orders of magnitude lower than $\sigma_{EP}$ and therefore contributes little to the overall long-range conductivity. In the case of the 700 EW


dx.doi.org/10.1021/ja3099799 | J. Am. Chem. Soc. 2013, 135, 822–834

membrane, the conductivity $\sigma_{IP}$ is within 1 and 3 orders of magnitude of $\sigma_{EP}$ and approaches $\sigma_{EP}$ with increasing temperature. In this membrane, the interfacial region gives a reasonably good percolation pathway for proton migration processes through the membrane and provides an alternative to the membrane-mediated $\sigma_{EP}$ process that exhibited the highest pseudo-activation energy of all the EWs. At the three lower EWs, $\sigma_{IP}$ follows an Arrhenius behavior indicating a proton hopping exchange process. However at 1000 and 1100 EW, $\sigma_{IP}$ shows a VTF trend, indicating that the dynamics of the membrane also facilitates the conduction along the interface between the hydrophobic and hydrophilic domains.

The conductivity values associated with the interfacial and electrode polarization phenomena determined from fitting the data of the wet membranes are plotted as a function of $1000/T$ in Figure 13. The conductivity at all EWs is at least 4 orders of magnitude higher than in the dry membranes at the highest temperatures. The increase in the conductivity can likely be attributed to both an increased charge concentration and mobility of the protons within the conductivity pathways in the membrane. The infrared spectroscopic results indicated that with even small amounts of water the covalently bonded protons are dissociated and delocalized from the sulfonate group.

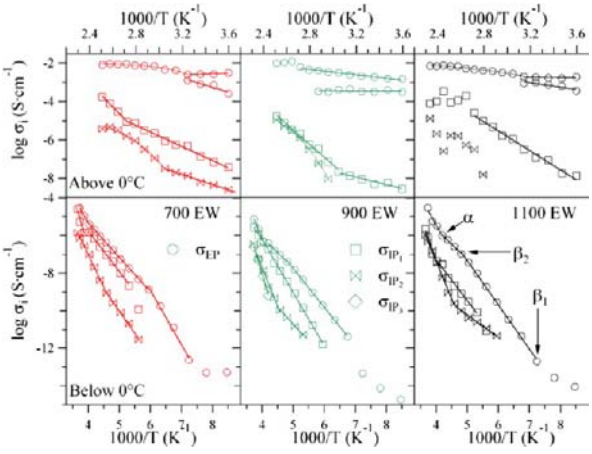


**Figure 13.** Log of conductivity as a function of $1000/T$ for select wet 3M membranes. The plots for the other equivalent weights is shown in the Supporting Information, Figure S13.

As discussed briefly above, the conductivity behavior becomes significantly more complicated in the wet membrane primarily due to the presence of multiple interfacial polarizations. These polarizations are the result of the presence of several different percolation pathways along the interfaces between the hydrophobic and water-swelled hydrophilic domains. These percolation pathways make varying contributions to the overall long-range conductivity depending on the temperature of the membranes.

Above the melting point of water, the electrode polarization has two contributions that merge into one as the temperature increases. It is hypothesized here that there are two types of hydrophilic domains that have different probabilities for ion exchange or contain different amounts of water and therefore provide different charge migration pathways. Initially, one domain is more favorable for proton conduction. As the temperature is increased and water moves between the domains, the difference between these pathways becomes smaller and they eventually merge into a single contribution. At higher temperatures, the electrode polarization exhibits VTF behavior for some EWs and an Arrhenius trend in others. The lack of a consistent trend as a function of EW suggests that the conduction mechanism is dominated by the fast exchange of protons between water clusters embedded in delocalization bodies (DBs). A DB is a volume of bulk membrane containing both the hydrophobic and hydrophilic domains that is identified by conduction pathways where the migrating charged species (in this case $H^+$) can be considered to be delocalized. In this scenario, charge exchange between coordination sites along the conduction pathways, defined by the DB volume itself, is much faster than charge transfer between DBs and therefore the charge is considered to be delocalized within the DB volume. Furthermore, the proton exchange process between contacting DBs may be somewhat facilitated by the dynamics of the host polymer in the hydrophobic domains.

Above 0 °C, the interfacial polarization phenomena have conductivity values that are at least 2 orders of magnitude smaller than the electrode polarization. For all of the EWs except 1000, there are two interfacial polarizations: one that shows Arrhenius behavior and another that follows a VTF trend. Therefore, it is reasonable to assume that protons are exchanged along the interface via migration processes between coordination sites that may be facilitated by the dynamics of the perfluorocarbon backbone chain of the 3M membranes. It should be noted that the interfacial conductivities $\sigma_{IP_1}$ and $\sigma_{IP_2}$ for the 1100 EW membrane were not fit due to the substantial scattering of the data at high temperatures, but the general trend seems to be consistent with the other EWs.

The overall long-range conductivity may be approximated as

$$\sigma_{TOT} = \sigma_{EP} + \sigma_{IP_1} + \sigma_{IP_2} \approx \sigma_{EP} \quad (4)$$

This approximation implies that while there is charge migration along the interface within the hydrophobic−hydrophilic domains, the exchange of protons between different hydrophilic domains is likely the rate-limiting step of the overall conduction process.

Below the melting point of water, the long-range conductivity has more than one significant contribution. As previously discussed, at least two conductivity contributions are present as indicated by two plateaus in the real part of the conductivity and the series of peaks in the tan $\delta$ spectra as a function of frequency. In contrast to the behavior above 0 °C, the overall long-range conductivity in the presence of crystallized water clusters should be considered the sum of the electrode and interfacial polarizations. This is particularly true for the 700 and 900 EW membranes, where $\sigma_{IP_1}$ is essentially equal to $\sigma_{EP}$ at temperatures close to 0 °C. In general, the $\sigma_{IP}$ conductivities make a larger contribution in the smaller EW membranes, likely due to the existence of a greater number of interfaces in the membrane due to the smaller hydrophobic domains and a higher number of polar side chains which reduces the hopping distances between proton coordination sites. The larger domains present in the higher EW membranes, as suggested by the XRD results, likely provide percolation pathways for charge migration and reduces the probability of charge transfer along the interface.

The conductivity $\sigma_{EP}$ can be divided into four different temperature regions delimited by molecular relaxations $\gamma$, $\beta_1$, and $\beta_2$ as demonstrated for the 1100 EW membrane in Figure 13. In all temperature regions below 0 °C and for all EWs, the


dx.doi.org/10.1021/ja3099799 | J. Am. Chem. Soc. 2013, 135, 822−834

data follow Arrhenius behavior, which suggests that proton migration occurs via hopping exchange processes between coordination sites. This result is not unexpected because below the $\alpha$ transition of the perfluorocarbon backbone and in the presence of crystallized water clusters within the hydrophilic domains, the dynamics of the membrane would likely be severely inhibited. The slope of the Arrhenius fit is proportional to the activation energy associated with the conduction process. The slope of the Arrhenius fit above the $\beta_2$ relaxation is smaller than the slope in the lower temperature region, which suggests that fluctuations of the side chain aid the proton exchange process. The opposite trend is observed above the $\alpha$ relaxation where there is an increase in the slope of the Arrhenius fit. This increased activation energy would imply that above the $\alpha$ relaxation the motion of the PTFE main chain in the presence of crystalline water hinders proton hopping.

The behavior of the parameters associated with the molecular relaxations evident in the permittivity and tan $\delta$ spectra (Figures 8 and 10, respectively) is shown in Figure 14 and Figure S14. For all EWs, the frequencies associated with the $\alpha$ relaxation can be fit with the VTF equation above approximately 0 °C. VTF behavior is typically expected for relaxations associated with the polymer backbone chain. The pseudo-activation energies found from the VTF fits are on the same order of magnitude as those found for the conductivities and frequencies associated with the $\sigma_{EP}$ of the dry membrane. This result suggests that the dynamics of the main polymer chain in the dry membrane is coupled with the charge exchange processes, which occur via hopping between coordination sites. The frequencies associated with the $\beta$ relaxations, as expected, exhibit Arrhenius behavior. It is interested to note that the activation energies at higher temperature increase from 66 to 148 kJ/mol with increasing membrane EW. This result suggests that a lower number of side chains and longer PTFE segments inhibit the $\beta$ relaxation mode due to an increase in the crystallinity in the hydrophobic domains that restricts the mobility of the side chains.

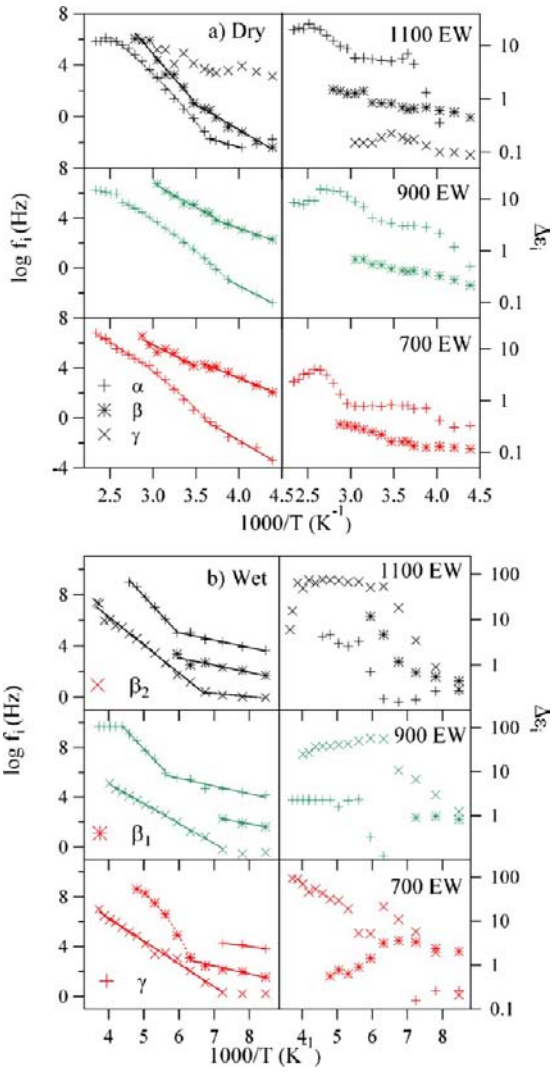


**Figure 14.** Log of the frequencies and the dielectric strengths associated the molecular relaxations for select 3M membranes: (a) dry and (b) wet. The plots for the other equivalent weights are shown in the Supporting Information.

The $\beta$ relaxation associated with the side chain in the dry membranes is separated into two individual contributions, $\beta_1$ and $\beta_2$, in the wet materials. The $\beta_1$ mode is attributed to fluctuations of the dipole of ether moieties and the $\beta_2$ relaxation is associated with fluctuations of the dipole of water-solvated sulfonate groups. The dielectric strength, $\Delta\varepsilon$, of the $\beta_2$ mode is more than an order of magnitude larger than the $\Delta\varepsilon$ of $\beta_1$. A dielectric strength as large that of $\beta_2$ (see Figure 14b) must be associated with a group with a very large dipole moment, such as a water-solvated sulfonate group. The relaxation frequencies associated with $\beta_2$ follow Arrhenius behavior with activation energies of between 30 and 45 kJ/mol for all EWs. These activation energies are very close to the activation energies associated with $\sigma_{EP}$ and $\sigma_{IP1}$ below the $\alpha$ relaxation, which suggests that the $\beta_2$ relaxation is closely associated with the long-range conduction mechanism below the melting point of water.

At lower temperatures, the $\beta_1$ and $\gamma$ modes follow Arrhenius behavior and have low and comparable activation energies. These activation energies are much smaller than those of $\beta_2$ which implies that $\beta_1$ and $\gamma$ likely do not have a substantial effect on the mechanism of charge transport. At higher temperatures, the combined $\beta_1$ + $\gamma$ peak exhibits a mix of VTF and Arrhenius behavior. In the EWs where VTF behavior occurs, the peak is likely dominated by the $\gamma$ transition. When an Arrhenius trend is seen, the largest contribution probably comes from the $\beta_1$ mode.

## ■ CONCLUSIONS

This study focuses on change in the 3M membrane structure as a function of the equivalent weight and the relationship between the structure and the properties of the membrane. Decreasing the EW of the material results in a higher density of side chains and therefore in a larger number of sulfonic acid groups. The WAXS results showed evidence of both non-crystalline and crystalline ordered hydrophobic regions in all the EW membranes except the 700 EW membrane, which suggests that a minimum PTFE segment length between adjacent side chains is necessary for the formation of crystalline hydrophobic domains. The non-crystalline domains are composed of ordered aggregates with a particle size of ca. 20 Å. In contrast, the crystalline region has crystallites of 95−115 Å in the dry membrane and 70−95 Å in wet conditions. The WAXS data suggest the chains of the 3M membranes in ordered domains primarily exist in small crystallites that have a diameter of about 20 Å, but in all but the lowest EWs there is


dx.doi.org/10.1021/ja3099799 | J. Am. Chem. Soc. 2013, 135, 822−834

also a small amount of larger crystallites with a diameter of about 100 Å. When there is water in the membrane, there is a decrease in the size of the larger domains and consequently a decrease in the overall crystallinity. This result suggests that some chains are released from the larger domains and either form smaller domains or contribute to the amorphous fraction.

The spectral changes evident in the vibrational spectra of the 3M membranes at different water contents can be associated with two major phenomena: (1) the dissociation of the proton from the sulfonic acid groups even in the presence of small amounts of water; and (2) the changes in the conformation or the degree of crystallinity of the PTFE hydrophobic domains both as a function of EW and membrane water content. The dissociation of the acidic proton is most evident by the intensity decreases at 1410 and 930 $cm^{-1}$ and the band growth at 1057 and 1288 $cm^{-1}$. The decrease of the bands between 1135 and 1147 $cm^{-1}$ is attributed to the loss of crystallinity of the PTFE hydrophobic domains evident in the WAXS spectra.

All membranes, regardless of EW, are thermally stable up to 360 °C. The DSC results of the dry membranes exhibit two thermal events: the $\beta$ transition likely associated with the ether moiety in the side chain between −40 and −55 °C and the $\alpha$ transition between 15 and 40 °C assigned to the $13_6 \rightarrow 15_7$ helix transformation and to the order−disorder conformational transitions[26,30,37] occurring in hydrophobic PTFE-like domains. The $\beta$ transition temperature generally decreases with an increased density of side chains in the membrane as the proximity between side chains allows more interactions between side chains. In contrast, the $\alpha$ transition has no clear trend as a function of EW.

The 3M membranes have conductivities between 7 and 20 mS/cm at 125 °C in the presence of water. In wet conditions above the melting point of water and in dry conditions above the $\alpha$ transition, the conductivity values follow VTF behavior, which suggests that the proton migration occurs via proton exchange processes between DBs that is facilitated by the dynamics of the host polymer. The results seen here are consistent with the other studies that show different morphological structures and improved electrical properties of short side chain ionomers as compared to Nafion at low EW.[24,38,47,48]

In the wet membrane above the melting point of water, the percolation pathway associated with the electrode polarization due to fast exchange processes between DBs is primarily responsible for the long-range conductivity. Immediately following the melting of water, the electrode polarization has two contributions that merge into one as the temperature increases. These contributions could originate from the presence of two types of ordered hydrophilic domains immersed in amorphous domains that have different probabilities for ion exchange or contain different amounts of water and therefore provide different charge migration pathways through the bulk of the hydrophilic domains. At higher temperatures where only a single event is visible, the electrode polarization exhibits VTF behavior for some EWs and an Arrhenius trend in others. The lack of a consistent trend as a function of EW suggests that the conduction mechanism is dominated by the fast exchange of protons between DBs; furthermore, these proton exchange processes may be somewhat facilitated by the morphology and the dynamics of the host polymer in the hydrophobic domains. In the wet membrane below the melting point of water, the long-range conductivity has more than one major contribution and therefore should be considered the sum of the electrode and interfacial polarizations. In the dry membranes, the conductivity associated with interfacial polarization, $\sigma_{IP}$, is several orders of magnitude lower than $\sigma_{EP}$ and therefore contributes little to the overall long-range conductivity in all EWs except for 700 EW.

The interfaces between domains are illustrated in Figure 15 for low and high EW membranes. The long-range conductivity occurs in the direction normal to the cross-section shown. The $\sigma_{IP}$ conductivities tend to make a larger contribution to the long-range conduction mechanism in the smaller EW membranes likely due to the existence of a greater number of interfaces in the membrane due to the smaller hydrophobic domains and a higher number of polar side chains which reduces the hopping distances between proton coordination sites. The larger domains present in the higher EW membranes, as suggested by the XRD results, likely provide percolation pathways for charge migration through the DBs and reduces the probability of charge transfer along the interface. Therefore, although there is charge migration along the interface within the hydrophobic−hydrophilic domains, the exchange of protons between different DBs is likely the rate-limiting step of the overall conduction process. Based on the hypothesized conduction mechanism, the morphology of the hydrophobic domains plays a crucial role in modulating long-range proton migration in the 3M membranes.

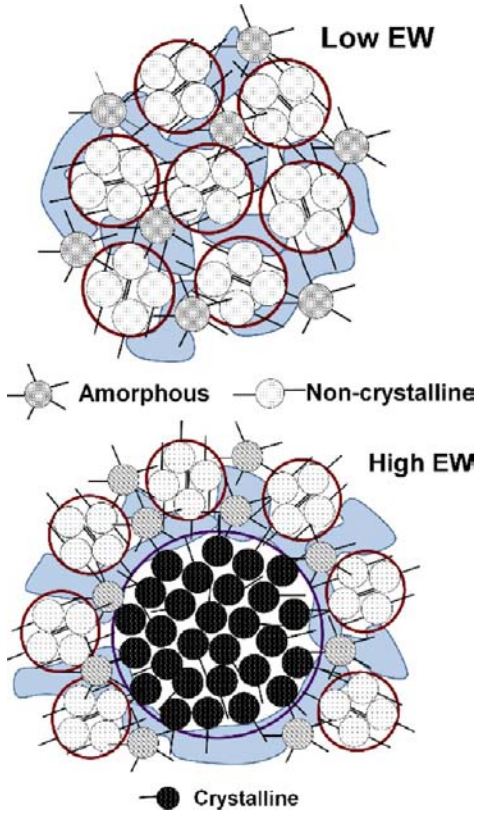


**Figure 15.** Interfaces between domains. The crystalline domains refer to the large crystallites that have an average size of 70−90 Å. The non-crystalline domains refer to smaller regions with crystallites that are approximately 20 Å. The amorphous regions are domains that exhibit no translational symmetry. Long-range proton transport occurs in the direction normal to the cross-section shown.


dx.doi.org/10.1021/ja3099799 | J. Am. Chem. Soc. 2013, 135, 822−834

## ■ ASSOCIATED CONTENT

### Supporting Information

Real part of the conductivity, real part of the permittivity and tan $\delta$ for all of the EW membranes; relaxation frequencies associated with the conductivity as a function of $1000/T$ for the dry 3M membranes; log of conductivity as a function of $1000/T$ for 825 and 1000 EW 3M membranes; log of the frequencies and the dielectric strengths associated the molecular relaxations for 825 and 1000 EW 3M membranes, both dry and wet; activation energies associated with the conductivity and relaxation phenomena. This material is available free of charge via the Internet at http://pubs.acs.org.

## ■ AUTHOR INFORMATION

### Corresponding Author

vito.dinoto@unipd.it

### Notes

The authors declare no competing financial interest.

## ■ ACKNOWLEDGMENTS

The authors thank Matteo Piga for assistance with the experimental work. G.G. thanks Regione del Veneto (SMUPR n. 4148, Polo di ricerca del settore fotovoltaico) for funding.

## ■ REFERENCES

(1) O'Hayre, R.; Cha, S. W.; Prinz, F. B. *Fuel Cell Fundamentals*; Wiley: Hoboken, NJ, 2006.
(2) Laberty-Robert, C.; Valle, K.; Pereira, F.; Sanchez, C. *Chem. Soc. Rev.* **2011**, *40*, 961.
(3) Doyle, M.; Rajendran, G. In *Handbook of Fuel Cells: Fundamentals Technology and Applications*; Vielstich, W., Lamm, A., Gasteiger, H. A., Eds.; John Wiley & Sons: Chichester, 2003; Vol. 3, p 351.
(4) Grot, W. *Fluorinated ionomers*; William Andrew: Norwich, NY, 2008.
(5) Satyapal, S. In *5th International Conference on Polymer Batteries & Fuel Cells*; US Department of Energy: Energy Efficiency & Renewable Energy: Argonne, IL, 2011.
(6) Epping, M. K.; Kopasz, J. P. *Fuel Cells* **2009**, *9*, 356.
(7) Mauritz, K. A.; Moore, R. B. *Chem. Rev.* **2004**, *104*, 4535.
(8) Gierke, T. D.; Munn, G. E.; Wilson, F. C. *J. Polym. Sci.: Polym. Phys. Ed.* **1981**, *19*, 1687.
(9) Rubatat, L.; Rollet, A. L.; Gebel, G.; Diat, O. *Macromolecules* **2002**, *35*, 4050.
(10) Schmidt-Rohr, K.; Chen, Q. *Nat. Mater.* **2008**, *7*, 75.
(11) Di Noto, V.; Piga, M.; Giffin, G. A.; Vezzù, K.; Zawodzinski, T. A. *J. Am. Chem. Soc.* **2012**, *134*, 19099.
(12) Hamrock, S. J.; Yandrasits, M. A. *Polym. Rev.* **2006**, *46*, 219.
(13) Aieta, N. V.; Stanis, R. J.; Horan, J. L.; Yandrasits, M. A.; Cookson, D. J.; Ingham, B.; Toney, M. F.; Hamrock, S. J.; Herring, A. M. *Macromolecules* **2009**, *42*, 5774.
(14) Liu, Y.; Horan, J. L.; Schlichting, G. J.; Caire, B. R.; Hamrock, S. J.; Haugen, G. M.; Yandrasits, M. A.; Seifert, S.; Herring, A. M. *Macromolecules* **2012**, *45*, 7495.
(15) Delley, B. *J. Chem. Phys.* **1990**, *92*, 508.
(16) Delley, B. *J. Chem. Phys.* **2000**, *113*, 7756.
(17) Fujimura, M.; Hashimoto, T.; Kawai, H. *Macromolecules* **1981**, *14*, 1309.
(18) Gierke, T. D.; Munn, G. E.; Wilson, F. C. *J. Polym. Sci., Polym. Phys. Ed.* **1981**, *19*, 1687.
(19) Norgaard, C. F.; Nielsen, U. G.; Skou, E. M. *Solid State Ionics* **2012**, *213*, 76.
(20) Rollet, A.-L.; Diat, O.; Gebel, G. *J. Phys. Chem. B* **2002**, *106*, 3033.
(21) Masetti, G.; Cabassi, F.; Morelli, G.; Zerbi, G. *Macromolecules* **1973**, *6*, 700.
(22) Painter, P. C.; Coleman, M. M.; Koenig, J. L. *The Theory of Vibrational Spectroscopy and its Application to Polymeric Materials*; Wiley: New York, 1982.
(23) Vainshtein, B. K. *Diffraction of X-rays by Chain Molecules*; Elsevier: Amsterdam, 1963.
(24) Kreuer, K. D.; Schuster, M.; Obliers, B.; Diat, O.; Traub, U.; Fuchs, A.; Klock, U.; Paddison, S. J.; Maier, J. *J. Power Sources* **2008**, *178*, 499.
(25) Klug, H. P.; Alexander, L. E. *X-Ray Diffraction Procedures For Polycrystalline and Amorphous Materials*, 2nd ed.; Wiley: New York, 1974.
(26) Clark, E. S. *Polymer* **1999**, *40*, 4659.
(27) Elliott, J. A.; Paddison, S. J. *Phys. Chem. Chem. Phys.* **2007**, *9*, 2602.
(28) Paddison, S. J. *J. New Mater. Electrochem. Syst.* **2001**, *4*, 197.
(29) Petersen, M. K.; Voth, G. A. *J. Phys. Chem. B* **2006**, *110*, 18594.
(30) Di Noto, V.; Piga, M.; Lavina, S.; Negro, E.; Yoshida, K.; Ito, R.; Furukawa, T. *Electrochim. Acta* **2010**, *55*, 1431.
(31) Di Noto, V.; Piga, M.; Negro, E.; Giffin, G. A.; Polizzi, S.; Zawodzinski, T. A. *Chem. Sci.* **2012**, sumbitted.
(32) Danilczuk, M.; Lin, L.; Schlick, S.; Hamrock, S. J.; Schaberg, M. S. *J. Power Sources* **2011**, *196*, 8216.
(33) Warren, D. S.; McQuillan, A. J. *J. Phys. Chem. B* **2008**, *112*, 10535.
(34) Lin-Vien, D.; Colthup, N. B.; Fately, W. G.; Grasselli, J. G. *The Handbook of Infrared and Raman Characteristic Frequencies of Organic Molecules*; Academic Press: San Diego, 1991.
(35) Zerbi, G.; Sacchi, M. *Macromolecules* **1973**, *6*, 692.
(36) Varetti, E. L. *Spectrochim. Acta, Part A* **1988**, *44A*, 733.
(37) Di Noto, V.; Boaretto, N.; Negro, E.; Giffin, G. A.; Lavina, S.; Polizzi, S. *Int. J. Hydrogen Energy* **2012**, *37*, 6199.
(38) Wu, D.; Paddison, S. J.; Elliott, J. A.; Hamrock, S. J. *Langmuir* **2010**, *26*, 14308.
(39) Brandrup, J.; Immergut, E. H.; Grulke, E. A. *Polymer Handbook*, 4th ed.; Wiley: New York, 1999.
(40) Giffin, G. A.; Piga, M.; Lavina, S.; Navarra, M. A.; D'Epifanio, A.; Scrosati, B.; Di Noto, V. *J. Power Sources* **2011**, *198*, 66.
(41) Di Noto, V.; Piga, M.; Pace, G.; Negro, E.; Lavina, S. *ECS Transactions* **2008**, *16*, 1183.
(42) Di Noto, V.; Giffin, G. A.; Vezzù, K.; Piga, M.; Lavina, S. In *Solid State Proton Conductors: Properties and Applications in Fuel Cells*; Knauth, P., Di Vona, M. L., Eds.; Wiley: Chichester, 2012.
(43) Fulcher, G. S. *J. Am. Ceram. Soc.* **1925**, *8*, 339.
(44) Tammann, G.; Hesse, W. *Z. Anorg. Allg. Chem.* **1926**, *156*, 245.
(45) Vogel, H. *Phys. Z* **1921**, *22*, 645.
(46) Ratner, M. In *Polymer Electrolyte Reviews 1*; MacCallum, J. R., Vincent, C. A., Eds.; Elsevier: London, 1987.
(47) Clark, J. K., II; Paddison, S. J. *Solid State Ionics* **2012**, *213*, 83.
(48) Clark, J. K., II; Paddison, S. J; Hamrock, S. J. *Phys. Chem. Chem. Phys.* **2012**, *14*, 16349.